Hindawi
International Journal of Aerospace Engineering
Volume 2023, Article ID 5534452, 13 pages
https://doi.org/10.1155/2023/5534452

Research Article

Effects of Key Structure of Pressure Swirl Nozzle on Atomization Performance

Tao Zhang,[1] **Junqi Chen**,[1] **Pan Wan**,[2] **Yong Wang**,[3] **and Rundong Li**[1]

[1]*School of Energy and Environment, Shenyang Aerospace University, Shenyang 110136, China*
[2]*Wuhan Maritime Communication Research Institute, Wuhan 430205, China*
[3]*Key Laboratory of Ocean Energy Utilization and Energy Conservation of Ministry of Education, Dalian University of Technology, Dalian 116023, China*

Correspondence should be addressed to Tao Zhang; zhangtao@sau.edu.cn

Received 22 February 2023; Revised 25 April 2023; Accepted 8 May 2023; Published 18 May 2023

Academic Editor: Tuo Han

The structure of the pressure swirl nozzle is the key factor affecting the atomization quality. Optimal design of nozzle structure is conducive to improving the atomization quality and has important significance for improving the efficiency and stability of the combustor. The effect of the swirl section diameter, the contraction section angle, the straight section diameter, and the expansion section angle on the spray cone angle and the liquid film thickness is studied by numerical simulation. The results show that the liquid film thickness and spray cone angle both decrease with the increase of the expansion section angle. As the straight section diameter increases, the spray cone angle and liquid film thickness both increased. Both the spray cone angle and the liquid film thickness have an optimal contraction angle value that is 60° and 45°, respectively. The increase in the ratio of the swirl section diameter to the straight section diameter can increase the liquid axial velocity. When the nozzle outlet has an expansion angle, the thickness of the liquid film is reduced. When the expansion section angle, the straight section diameter, the contraction section angle, and the swirl section diameter of the nozzle is 30°, 4 mm, 45°, and 12 mm, respectively, the atomization performance of this nozzle is the best.

1. Introduction

Pressure swirl nozzle is widely used in the fields of petrochemical industry, agriculture, fire extinguishing, and engine, because of its simple structure, low energy consumption, and good atomization quality. The structure of the pressure swirl nozzle is mainly composed of a swirl section, a contraction section, an equal straight section, and an expansion section. The atomization quality directly affects the combustion efficiency and stability of the engine combustion chamber [1]. There are many parameters that affect nozzle atomization performance. Zhang et al. [2] enhanced nozzle atomization quality under different fuel ratio. Guo et al. [3] explored the influence of environmental pressure change on nozzle spray cone angle. The structure of the nozzle is one of the key factors affecting the atomization quality, so it is of great significance to study the influence of the structure of the nozzle on the spray characteristics to improve the atomization quality of the fuel.

Jiang et al. [4] made predictions about the atomizing characteristic parameters using a combination of theoretical formulations and experimental investigation and pointed out the nozzles with the smallest atomizing droplet size. Sun et al. [5] carried out experimental research on air-blast nozzle to explore its atomization quality and variation rule under different working conditions. Zhang et al. pointed out the optimal working condition under different pressures and nozzle diameters [6]. By theoretical and practical methods, the research of Lv et al. yielded the empirical formula between the spray cone angle and the Reynolds number [7]. Gad et al. [8] explored the influence of different dimensionless parameters such as the orifice length/

diameter ratio (Lo/Do), the swirl chamber length/diameter ratio (Ls/Ds), and the swirling passage size on the spray characteristics of the pressure swirl atomizer with/without assisted air. The results show that the spry angle of the nozzle decreases with the increase of Lo/Do or the decrease of air mass flow rate, the breakup length can be reduced by decreasing Ls/Ds, and the SMD can be reduced with the increase of gas assistance.

Although the experiment is the most direct method to explore the nozzle spray characteristics, with the development of computer technology and the gradual improvement of theoretical models, numerical simulation has gradually become one of the economical and effective methods to explore the spray characteristics. In theoretical research, Fu et al. [9] calculated the amplitude-frequency transfer characteristics of the indoor oscillation of a dual-component nozzle as it changes with the fuel mixing ratio. The model can provide a better reference for engineering design. Yang et al. [10] explored the influence of structural parameters of an open-end swirl nozzle on the characteristics of the nozzle and showed that the oscillation phase could be delayed with the increase of the length of the swirl cavity to achieve the effect of the oscillation damper. Based on the VOF method, Liu et al. [11] conducted a single-factor variable study on the influence of the structure of the pressure swirl nozzle on the atomization quality, and besides, they analyzed the influence degree of different structures on the nozzle spray characteristics through the dimensionless influence factor and pointed out the key structural parameters affecting the nozzle atomization performance. It provided a reference for the subsequent optimization of the nozzle structure. With variation of the nozzle inlet number, the swirl chamber length, and nozzle diameter, Khani Aminjan et al. [12, 13] observed the influence of liquid film thickness, atomization spry angle, and SMD on the performance of pressure swirl nozzles with spiral inlet and tangential inlet. The simulation results are in good agreement with the experimental results, which proves that the method can accurately predict the atomization performance inside and outside the design point of nozzles. Qiao et al. [14] explored the influence law of nozzle structure parameters on biological fuel atomization quality through numerical simulation and fitted the flow discharge coefficient formula based on the empirical formula. Pan et al. [15] studied the influence of the position and angle of the inclination angle of the tangential groove on the atomization quality, pointed out the influence law of the structure on the spray cone angle and droplet size, and obtained the best combination of atomization quality under different structures. Zhao et al. [16] carried out a numerical simulation on the pressure swirl nozzle with a round platform at the nozzle top and studied the spray characteristics under different structural parameters, which had guiding significance for improving the atomization quality of the nozzle and the efficiency of seawater desalination.

It is necessary to achieve the best atomization performance of the nozzle under the combination of various factors in practice because most prior research concentrated on the nozzle atomization quality with a single variable. Khani Aminjan et al. [12] carried out nine experiments to consider the influence of the combination of two variables and three levels on the atomization quality. In order to consider the influence of the combination of multiple factors on the atomization quality of the pressure swirl nozzle, a large number of experiments are needed, which not only requires a large workload but also a high experiment cost. Orthogonal experiment can reduce the number of experiments as much as possible without affecting the experimental effect and effectively solve the problem caused by too many factors and levels [17]. Qiu et al. [18] optimized the nozzle structural parameters and explored the influence rule of nozzle outlet diameter, length of straight section, divergent angle, and divergent length on atomization quality parameters by orthogonal experiment. Zhao et al. [19] analyzed the influence of gas pressure, the outlet length of the nozzle, the size of the gas ring gap, and other parameters on the ejection spray volume through orthogonal experiments. Bai et al. [20] optimized the structure of the nozzle with swirl grooves and explored the influence laws of expansion angle, length of straight section, rise swirl groove angle, and number of swirl groove on atomization quality. However, in addition to the above structural parameters, a single structural variable shows that the parameters of the swirl section and the contraction section also have a great influence on the atomization quality of the nozzle.

In this paper, the overall structure of the pressure swirl nozzle is optimized to improve the atomization quality, and the multifactor structure combination of the nozzle was tested by the method of orthogonal experiment and numerical simulation. Song [21] pointed out that the outlet length and the total length of the nozzle had little influence on the flow of the pressure swirl nozzle. Therefore, the key parameters of the pressure swirl nozzle, such as the swirl section diameter, the contraction section angle, the equal straight section diameter, and the expansion section angle, are selected to explore the influence of the structure on the atomization quality of the nozzle, and the optimal structure combination and variation rule of atomization quality are obtained. The results are provided for the nozzle structure optimization to achieve the desired optimal atomization quality.

2. Computational Model and Method

2.1. Physical Model. A pressure swirl nozzle structure is shown in Figure 1. The structure of the pressure swirl nozzle is mainly composed of a swirl section, a contraction section, an equal straight section, and an expansion section. This study only focuses on the influence of the nozzle structure on the atomization quality, so the external flow field is not considered, and only the internal structure of the nozzle is modeled. Its specific dimensions are shown in Table 1.

2.2. Numerical Calculation Method. Fluent is employed to simulate transient flow in nozzle. The gas phase in this model is set as air, and the liquid is water. The VOF model is employed to track the interface. The model equation is as follows:

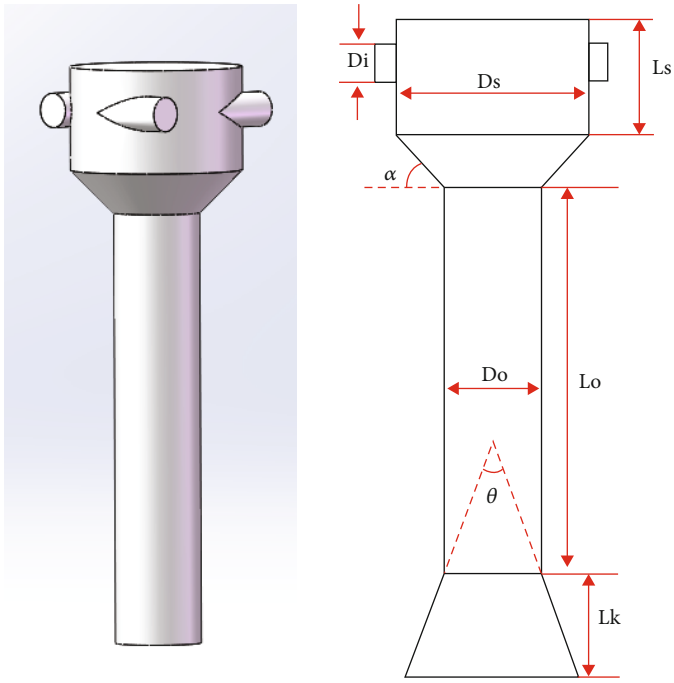

(a) 3D model of pressure swirl nozzle (b) Scale of pressure swirl nozzle

Figure 1: 3D model and scale of pressure swirl nozzle.

Table 1: Structure size of nozzle.

Parameter	Value
Tangential inlet diameter D_i/mm	2
Diameter of swirl chamber D_s/mm	10
Length of swirl chamber L_s/mm	6
Angle of contraction α/°	45
Diameter of equal straight section D_o/mm	5
Length of equal straight section L_o/mm	20
Angle of expansion section θ/°	0
Length of expansion section L_k/mm	5

Equation of continuity

$$\frac{\partial \alpha}{\partial t} + \nabla \bullet \alpha u = 0, \tag{1}$$

where α is the volume fraction. u is the velocity.

The momentum equation is solved in the whole computational domain, and the calculated velocity is the common velocity of the gas phase and the liquid phase, and its expression is

$$\frac{\partial \left(\rho \vec{v}\right)}{\partial t} + \nabla \bullet \left(\rho \vec{v}\,\vec{v}\right) = -\nabla p + \nabla \bullet \left[\mu\left(\nabla \vec{v} + \nabla \vec{v}^{T}\right)\right] + p\vec{g} + \vec{F}, \tag{2}$$

where ρ is the fluid density. p is hydrostatic pressure. μ is the dynamic viscosity. g is the acceleration of gravity. F is the external volume force, here referred to as surface tension.

Compares with the standard model, RNG $k-\varepsilon$ model not only takes into account the influence of swirl on turbulence but also can apply to a wide range of Reynolds number. The model can be expressed as follows:

$$\frac{\partial}{\partial t}(\rho k) + \frac{\partial}{\partial x_i}(\rho k u_i) = \frac{\partial}{\partial x_j}\left(\alpha_k \mu_{\text{eff}} \frac{\partial k}{\partial x_j}\right) + G_k + G_b - \rho\varepsilon - Y_M + S_k, \tag{3}$$

$$\frac{\partial}{\partial t}(\rho \varepsilon) + \frac{\partial}{\partial x_i}(\rho \varepsilon u_i) = \frac{\partial}{\partial x_j}\left(\alpha_\varepsilon \mu_{\text{eff}} \frac{\partial \varepsilon}{\partial x_j}\right) + C_{1\varepsilon}\frac{\varepsilon}{k}(G_k + C_{3\varepsilon}G_b) - C_{2\varepsilon}\rho\frac{\varepsilon^2}{k} - R_\varepsilon + S_\varepsilon, \tag{4}$$

where k is turbulence kinetic energy. ε is the turbulence diffusion rate. μ_{eff} is the effective viscosity. G_k and G_b represent the generation of turbulence kinetic energy due to the mean velocity gradients and the generation of turbulence kinetic energy due to buoyancy, respectively. Y_M is the dissipation rate generated by the wave expansion in compressible turbulence. This model assumes that the fluid is an incompressible flow, so here, $Y_M = 0$. α_k and α_ε are the reciprocal of valid Prandtl numbers k and ε. S_k and S_ε indicate the user-defined source item. $C_{1\varepsilon} = 1.42$, $C_{2\varepsilon} = 1.68$, and $C_{3\varepsilon} = 0.09$.

2.3. Boundary Conditions. The inlet boundary condition is set as the velocity inlet, and the inlet velocity is 18.46 m/s, and the volume fraction of the fluid is set as 1. The outlet boundary condition is set to the pressure outlet, and the outlet pressure is 0. The wall conditions are set to no slip and adiabatic wall conditions. The flow field is initialized with

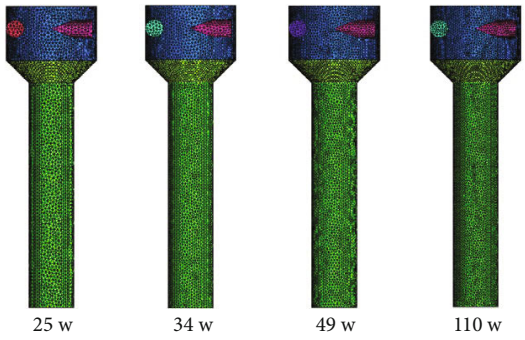

Figure 2: Meshing of the numerical solution domain.

the inlet boundary conditions, and besides, the liquid velocity of the computational domain and the volume fraction of water are set to 0.

2.4. Grid Independence Verification. As shown in Figure 2, the calculation area of the pressure swirl nozzle is divided into four different numbers of grids, 25 w, 34 w, 49 w, and 110 w, respectively. The variation of circumferential velocity at the outlet is used to verify the mesh independence, and the liquid film thickness obtained from the simulation results is compared with the theoretical liquid film thickness formula [22] to verify the calculated results.

In the simulation results, the isoline with the gas phase volume fraction of 0.5 is taken as the gas-liquid interface. The liquid film thickness is the distance between the wall surface and the isoline, and the gas core is the distance between the isoline, and the nozzle center liquid film thickness is expressed as

$$h_{lf} = r_w - r_{ac}, \tag{5}$$

where h_{lf} is the thickness of the liquid film. r_w is the radius of the nozzle outlet. r_{ac} is the radius of the gas core.

The theoretical liquid film thickness is predicted by Lefebvre and Suyari [22], and it is expressed as

$$h_{lf} = 3.66\left(\frac{D_0 m\mu}{\rho\Delta p}\right)^{0.25}, \tag{6}$$

where D_0 is the nozzle outlet diameter. m is the mass flow rate. Δp is the pressure difference between inlet and outlet.

Mass flow formula

$$m = \rho VA = \rho V_a \pi D h_{lf}, \tag{7}$$

where V_a is the axial velocity. D is the nozzle diameter at the liquid film thickness section. h_{lf} is the liquid film thickness.

It can be seen from Figure 3 that the model with a mesh number of 49 w and 110 w can capture the circumferential velocity more accurately. It can be seen from Table 2 that the simulated values and empirical formula values of liquid film thickness calculated by Equation (5) and Equation (6) are basically unchanged, and the error is 5.2% and 5.3%, indicating that the mesh number of 49 w is sufficient to meet the calculation requirements [23]. All subsequent grids are divided with the parameter of 49 w mesh number.

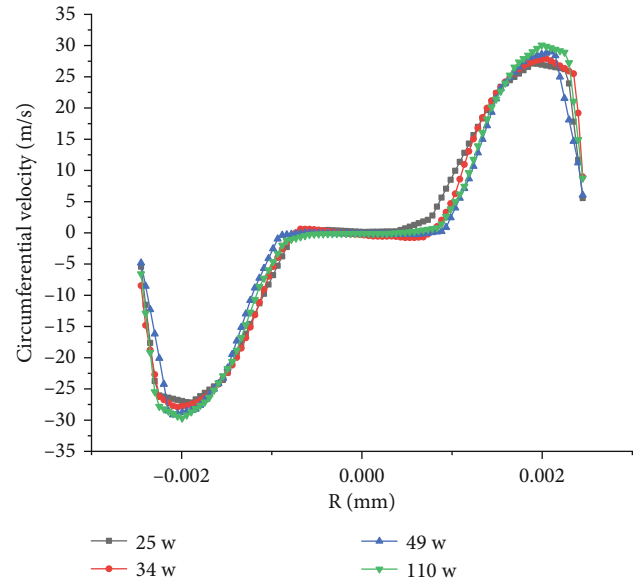

Figure 3: Circumferential velocity at the exit.

Table 2: Comparison of liquid film thickness between simulation results and empirical formula.

Number of grids	Simulation results	Empirical formula results	Error
25 w	0.671 mm	0.617 mm	8.0%
34 w	0.666 mm	0.621 mm	6.8%
49 w	0.655 mm	0.622 mm	5.2%
110 w	0.657 mm	0.624 mm	5.3%

3. Results and Discussion

According to the single-factor analysis [11, 14, 15], the swirl section diameter, the contraction section angle, the equal straight section diameter, and the expansion section angle have a great influence on the atomization quality of the pressure swirl nozzle. In Table 3, *A*, *B*, *C*, and *D* are represented as expansion angle, equal straight section diameter, contraction angle, and swirl section diameter, respectively. The four factors are taken into account in the orthogonal experiment, and a blank factor E, which carries out the variance analysis of subsequent data, is set to make the freedom of the experiment, not zero. The design of the orthogonal experiment refers to the orthogonal experiment table L_{16}, which means 16 structures. The nozzle structures are optimized to achieve better atomization performance by the liquid film thickness and spray cone angle.

3.1. Spray Cone Angle. The spray cone angle is calculated by Equation (8), and the velocity is calculated from the contours of the gas phase volume fraction of 0.25 [24]. The spray cone angle is shown in Figure 4.

Table 3: Experimental factors and levels.

Level	Factors				
	A Expansion angle/°	*B* Equal straight section diameter/mm	*C* Contraction angle/°	*D* Swirl section diameter/mm	*E* Blank
1	0	4	30	9	
2	10	5	45	10	
3	20	6	60	11	
4	30	7	75	12	

The spray cone angle formula is express as

$$\cos\frac{\beta}{2} = \frac{V_a}{U}, \tag{8}$$

where U is the liquid total velocity. V_a is the liquid axial velocity.

Table 4 shows the orthogonal experimental results of the spray cone angle under the value of the corresponding factor. R is the range, which reflects the influence of various factors on the index. The larger R means the greater the degree of influence. It can be seen from the results that $R_A > R_B > R_D > R_C$, indicating that the influence degree of each factor on the spray cone angle is successively the expansion section angle, the equal straight section diameter, the swirl section diameter, and finally, the contraction section angle. K_i is the sum of the level test values of a factor, which can be used to judge the merits of the level and combination. The expansion section result shows that the order of K value is $K_{A1} > K_{A2} > K_{A3} > K_{A4}$, and the K values of other factors are $K_{B4} > K_{B3} > K_{B2} > K_{B1}$, $K_{C3} > K_{C2} > K_{C1} > K_{C4}$, and $K_{D2} > K_{D4} > K_{D3} > K_{D1}$. Spray cone angle plays a great influence on gas-liquid interaction and is an important factor affecting atomization quality. With the increase of spray cone angle, the larger the area of fuel and gas mixing. According to the above K value, it can be concluded that the structure combination with the largest spray cone angle is $A_1B_4C_3D_2$. When the expansion section angle is 0°, the equal straight section diameter is 7 mm, the contraction section angle is 60°, and the swirl section diameter is 10 mm; the spray cone angle of this nozzle is the largest of all.

Table 5 shows the variance results of the orthogonal experiment. The sum of the squares of deviation is the sum of the squares of the differences between the values of the factors and their means. The mean square is the ratio of the sum of the squares of deviation to the degrees of freedom. F is the ratio of mean square deviation to mean square deviation of error. P value is a parameter used to determine the significance of the calculated results. When $P \le 0.01$, $0.01 \le P \le 0.05$, and $P \ge 0.05$, they mean that the factor has an extremely significant, a significant, and no significant impact on the results, respectively. As can be seen from Table 5, the P values of the expansion section angle and the equal straight section diameter are 1.54E-05 and 7.97E-05, respectively, indicating that the expansion section angle and the equal straight section diameter have an extremely significant influence on the spray cone angle. The P values of the contraction section angle and the swirl section diameter are 0.943 and 0.110, respectively, indicating that the factor has no significant effect on the spray cone angle.

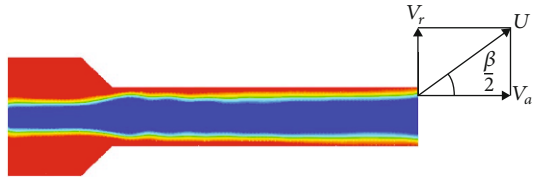

Figure 4: Spray cone angle schematic figure.

Figure 5 shows the variation of the spray cone angle with different factors and levels. It can be seen from Figure 5(a) that the spray angle decreases gradually with the increase of the expansion angle, which is consistent with the reference [25]. This is due to the wall-sticking effect. There exists an expansion angle in the nozzle outlet that can reduce the spray cone angle [25]. Figure 5(b) shows that as the equal straight section diameter increases, the spray cone angle increases, which is consistent with Qiu et al. [18]. According to the classic pressure swirl nozzle theory [26], the geometry characteristic constant denotes the swirl intensity of the liquid ejected from the swirl nozzle. The geometry characteristic constant increases with increased nozzle diameter. So, the liquid swirled more intensely when it was ejected from the nozzle, and a larger spray cone angle should be formed from an injector with a larger nozzle diameter [27, 28]. Figure 5(c) shows that there exists an optimal contraction section angle value such that the spray cone angle is maximum. When the contraction section angle is less than 60°, the increase of the contraction section angle leads to the increase of the fluid swirl velocity through the contraction section. That led to the spray cone angle increases according to Equation (8). When the contraction section angle is greater than 60°, the contraction section angle becomes larger, and the fluid forms a reflux area in the contraction section, resulting in velocity loss and a smaller spray cone angle [14]. From Figure 5(d), it can be seen that the spray cone angle increases with the swirl section diameter and then fluctuates up and down as the diameter increases. The swirl section diameter increases, and the liquid swirl intensity in the swirl chamber increases so that the spray cone angle increases. However, as the swirl section diameter increases, the nozzle local friction loss also increases, resulting in a reduction in spray cone angle. The fluctuation of the spray cone angle is the result of the alternating effects of swirl intensity and local friction loss.

Table 4: Orthogonal experimental results of spray angle.

Number	A/°	B/mm	C/°	D/mm	E	Spray cone angle/°
1	0	4	30	9	1	83.55
2	0	5	45	10	2	94.39
3	0	6	60	11	3	100.82
4	0	7	75	12	4	105.66
5	10	4	45	11	4	60
6	10	5	30	12	3	71.1
7	10	6	75	9	2	75.58
8	10	7	60	10	1	82.73
9	20	4	60	12	2	52.95
10	20	5	75	11	1	61.44
11	20	6	30	10	4	68.42
12	20	7	45	9	3	72.93
13	30	4	75	10	3	51.44
14	30	5	60	9	4	58.56
15	30	6	45	12	1	66.79
16	30	7	30	11	2	71.08
R	34.14	20.97	0.24	1.59	—	—
K_1	384.42	248.51	294.15	280.62	—	—
K_2	289.98	285.49	294.68	296.98	—	—
K_3	255.74	311.61	295.06	293.91	—	—
K_4	247.87	332.40	294.12	296.50	—	—
k_1	96.11	62.13	73.54	72.66	—	—
k_2	72.50	71.37	73.67	74.25	—	—
k_3	63.94	77.90	73.77	73.48	—	—
k_4	61.97	83.10	73.53	74.13	—	—

Table 5: Variance analysis of spray angle.

Source of variance	Sum of squares of deviation	Degree of freedom	Mean square	F	P
A	2945.68	3	981.894	2302.09	1.54E-05
B	981.36	3	327.119	766.94	7.97E-05
C	0.15	3	0.051	0.12	0.943
D	6.39	3	2.129	4.99	0.110
E (error)	1.28	3	0.427	—	—

3.2. Liquid Film Thickness. The thinner liquid film thickness can obtain the better atomization quality [29, 30]. Table 6 shows the orthogonal experiment results of liquid film thickness at the nozzle outlet. It can be seen from the range R that $R_A > R_B > R_D > R_C$, indicating that the most important factor affecting the liquid film thickness is the expansion section angle, followed by the equal straight section diameter, then the contraction section angle, and the swirl section diameter. From the liquid film thickness index K_i, it can be seen that $K_{A1} > K_{A2} > K_{A3} > K_{A4}$, $K_{B4} > K_{B3} > K_{B2} > K_{B1}$, $K_{C4} > K_{C3} > K_{C1} > K_{C2}$, and $K_{D1} > K_{D2} > K_{D3} > K_{D4}$. The liquid film thickness index results show that the $A_4B_1C_2D_4$ is the structural combination with the minimum liquid film thickness of nozzle, indicating that the liquid film thickness is the minimum when the expansion section angle is 30°, the equal straight section diameter is 4 mm, the contraction section angle is 45°, and the swirl section diameter is 9 mm.

Table 7 shows the variance analysis results of liquid film thickness. It can be seen that the P value of the expansion section angle is 1.13E-04, indicating that the expansion section angle has an extremely significant influence on the liquid film thickness. The P value of the equal straight segment diameter is 0.012286, indicating that the equal straight segment diameter has a significant effect on the liquid film thickness. The P values of the contraction section angle and swirl section diameter are 0.19375 and 0.19375,

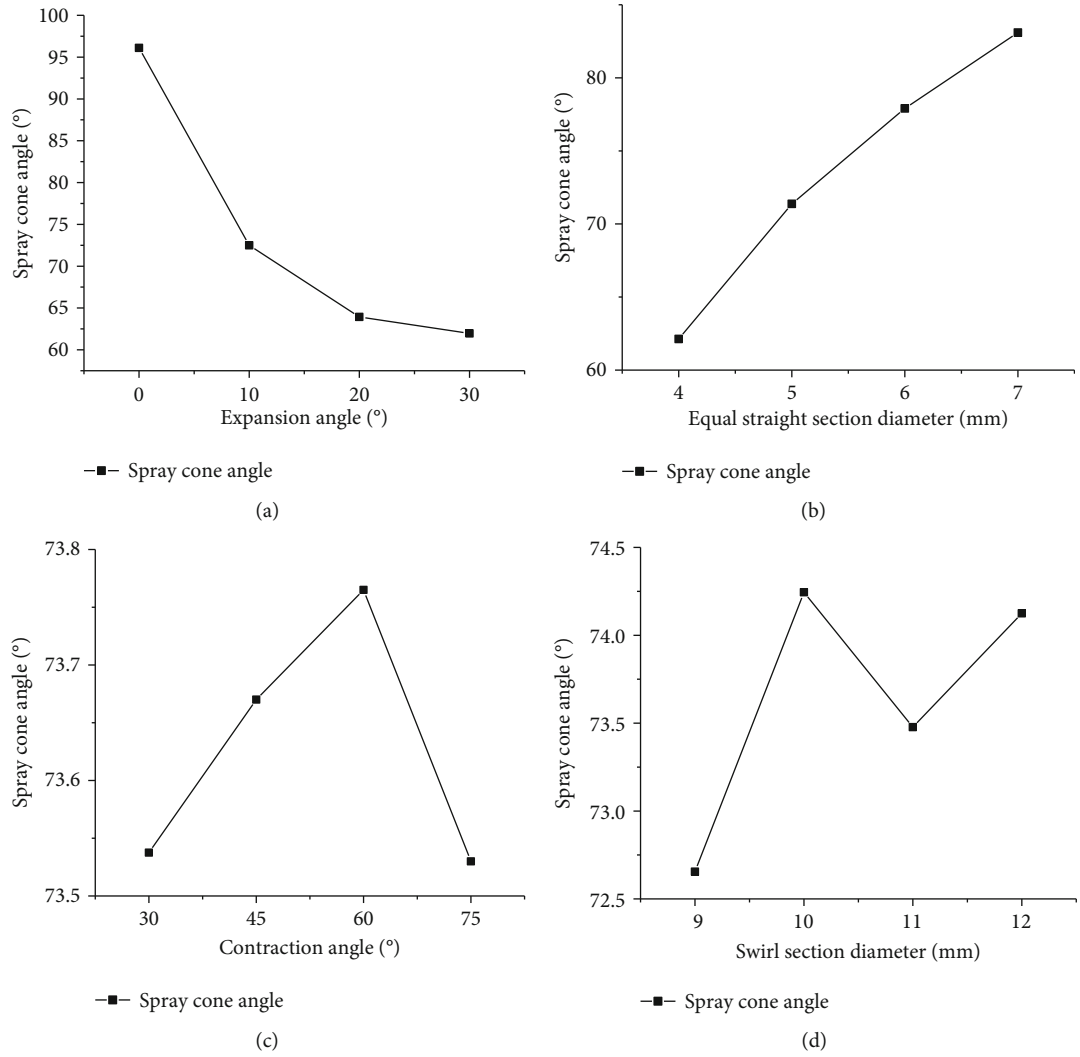

Figure 5: The relationship between k_i and spray cone angle at different levels of various factors.

respectively, indicating that the contraction section angle and swirl section diameter have no significant effect on the nozzle liquid film thickness.

Figure 6 shows the relationship between k_i and liquid film thickness at different factor levels. It can be seen from Figure 6(a) that when mass flow keeps constant, increasing the outlet expansion angle causes an increase in the liquid velocity and a decrease in the liquid film thickness at the nozzle outlet. But the variation trend slows down gradually, which is consistent with this reference [31]. Figure 6(b) shows that the liquid film thickness increases as the equal straight section diameter increases. This result was documented by other investigation of hollow-cone sprays from pressure swirl nozzles [30]. The larger the outlet diameter, the smaller variation in the section area of the nozzle from the swirl section to the outlet; the fluid kinetic energy loss becomes smaller, and the liquid film generated in the swirl section is less influenced. The liquid film thickness reaches the minimum value under the condition of an optimum value of the contraction section angle. It can be concluded from Figure 6(c) that the liquid film thickness reaches the minimum under the condition of an optimum value of the contraction section angle. The reason is similar to the relation between the spray cone angle and the contraction section angle. Figure 6(d) shows that the liquid film thickness decreases with the increase of swirl section diameter. The liquid swirl strength in the nozzle increases as the swirl section diameter. Under more sufficient centrifugal force, the liquid film thickness becomes thinner [32].

3.3. Structure Optimization and Comparative Analysis. Figure 7 compares the liquid phase volume fraction of the original structure with the structure combination with the minimum thickness of the liquid film. Figure 8 shows the variation of the gas core radius, liquid film thickness, and the liquid phase axial velocity as nozzle height. Figure 8 shows that the ratio of D_s/D_0 of $A_4B_1C_2D_4$ is larger than $A_1B_2C_2D_2$, and the cross-sectional area of fluid transitioning from the swirl section to the equal straight section changes more greatly, resulting in higher velocity after the fluid enters the equal straight section. The liquid film thickness in the equal straight section of $A_1B_2C_2D_2$ is about 0.8 mm,

Table 6: Orthogonal experimental results of liquid film thickness.

Number	A/°	B/mm	C/°	D/mm	E	Liquid film thickness/mm
1	0	4	30	9	1	0.664
2	0	5	45	10	2	0.655
3	0	6	60	11	3	0.673
4	0	7	75	12	4	0.704
5	10	4	45	11	4	0.385
6	10	5	30	12	3	0.413
7	10	6	75	9	2	0.487
8	10	7	60	10	1	0.491
9	20	4	60	12	2	0.309
10	20	5	75	11	1	0.366
11	20	6	30	10	4	0.368
12	20	7	45	9	3	0.422
13	30	4	75	10	3	0.333
14	30	5	60	9	4	0.343
15	30	6	45	12	1	0.333
16	30	7	30	11	2	0.364
R	0.331	0.073	0.024	0.039	—	—
K_1	2.696	1.691	1.809	1.916	—	—
K_2	1.776	1.777	1.795	1.847	—	—
K_3	1.465	1.861	1.816	1.788	—	—
K_4	1.373	1.981	1.890	1.759	—	—
k_1	0.674	0.423	0.452	0.479	—	—
k_2	0.444	0.444	0.449	0.462	—	—
k_3	0.366	0.465	0.454	0.447	—	—
k_4	0.343	0.495	0.473	0.440	—	—

Table 7: Variance analysis of liquid film thickness.

Source of variance	Sum of squares of deviation	Degree of freedom	Mean square	F	P
A	0.27373	3	0.09124	609.31	1.13E-04
B	0.011467	3	0.00382	25.52	0.012286
C	0.001359	3	0.00045	3.03	0.19375
D	0.003616	3	0.0012	8.05	0.060251
E (error)	0.000449	3	0.00015	—	—

while the liquid film thickness in the equal straight section of $A_4B_1C_2D_4$ is about 0.659 mm. Compared with $A_1B_2C_2D_2$, the liquid film thickness in the equal straight section of $A_4B_1C_2D_4$ is thinner. As the liquid enters the expansion section, the outlet diameter of $A_4B_1C_2D_4$ increases linearly from 2 mm to 3.35 mm, and the liquid axial velocity at the gas-liquid boundary increases from 35.23 m/s to 47.66 m/s. It can be seen from Equation (7) that when the liquid mass flow rate remains unchanged, with the increase of the outlet diameter and axial velocity, liquid film thickness decreases.

The original structure is compared with the structure combination with the largest spray cone angle. Figure 9 shows the velocity change curve at the gas volume fraction of 0.25 compared with the nozzle of the original structure; $A_1B_4C_3D_2$ has a smaller D_s/D_0 and a larger angle of the contraction section so that the fluid transition from the swirl section to the equal straight section is smoother. The fluid axial velocity increased by increasing D_s/D_0. In the nozzle outlet with an expansion angle, the axial velocity can be increased further. Figure 9 shows that the V_a/U of $A_1B_2C_2D_2$ is less than that of $A_1B_4C_3D_2$. As the liquid is supplied to the contraction section, the V_a/U of the $A_1B_2C_2D_2$ is larger than that of $A_1B_4C_3D_2$ after entering the contraction section due to V_a fluctuations near the inlet. According to Equation (8), the larger V_a/U is, the smaller the spray cone angle will be.

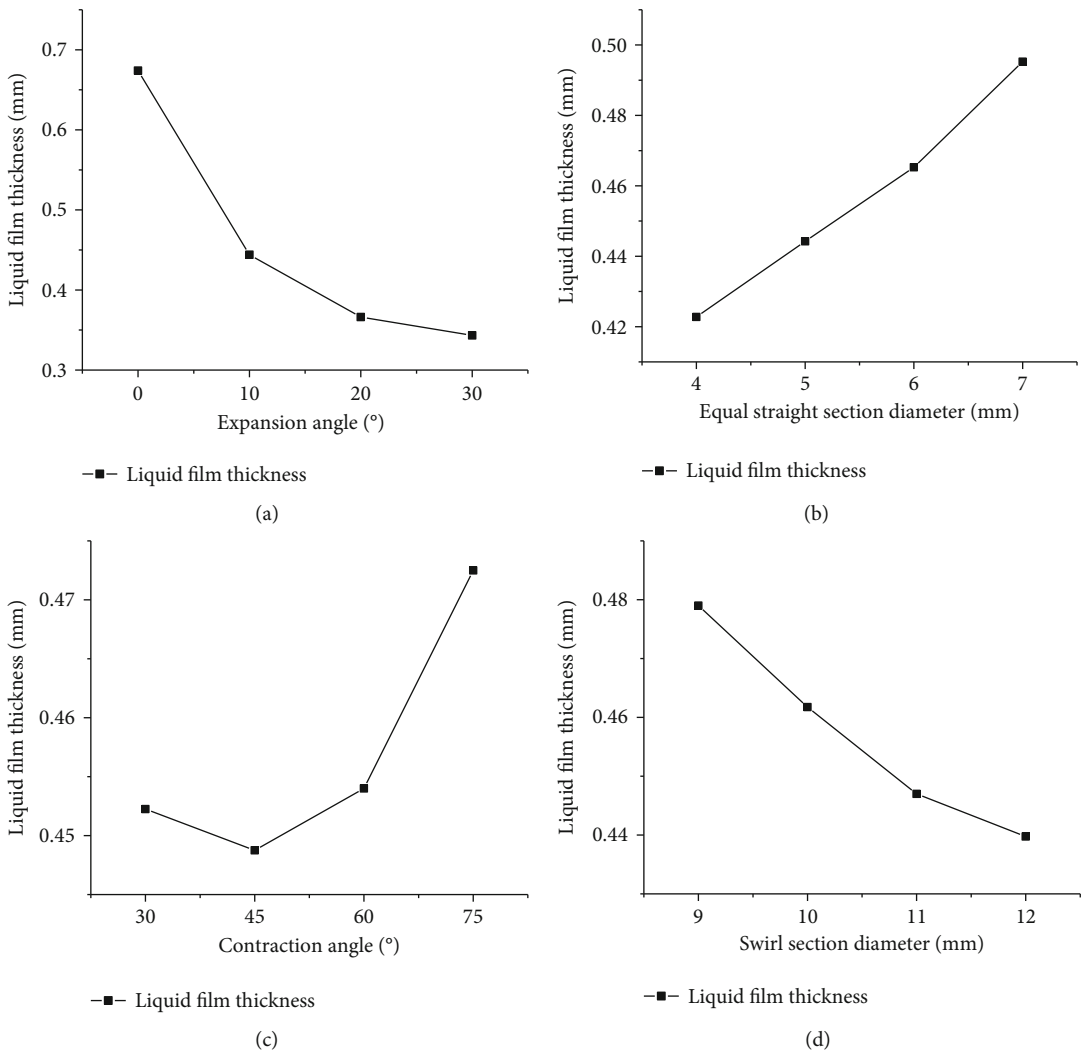

Figure 6: The relationship between k_i and liquid film thickness at different levels of various factors.

For small-diameter combustor, in order to prevent fuel droplets from ejecting to the wall and causing insufficient combustion and carbon deposition, the spray cone angle is generally about 50-80° [33]. The spray cone angle and liquid film thickness of $A_1B_2C_2D_2$ are 94.39°and 0.655 mm, respectively. The spray cone angle should be reduced to satisfy the small-diameter combustor. The contraction section angle and the swirl section diameter have no significant effect on the spray cone angle and liquid film thickness. So the swirl section diameter is set as 12 mm to reduce the liquid film thickness from Figure 6(d). The contraction section angle increases from 45° to 60°, the K_i of spray cone angle increases from 73.50° to 74.07° with a growth rate of 0.78%, and the K_i of liquid film thickness decreases from 0.454 to 0.460 with a growth rate of 1.32%. When the contraction section angle is 45°, the atomization quality is better. With the increase of the equal straight section diameter, the spray cone angle and liquid film thickness increase, and the Sauter mean diameter (SMD) also increases [21, 32]. Therefore, when the equal straight section diameter is 4 mm, the atomization quality is better, and the liquid film thickness and the spray cone angle decrease.

The expansion section angle has a very significant influence on the spray cone angle and liquid film thickness, so it is necessary to further optimize the expansion section angle through a single variable to achieve the best atomization quality. The atomization quality of the four nozzle $A_1B_1C_2D_4$, $A_2B_1C_2D_4$, $A_3B_1C_2D_4$, and $A_4B_1C_2D_4$ with the different expansion section angle is compared with each other. But liquid film thickness and spray cone angle cannot be assessed separately for atomization quality. Fortunately, Equation (9) fully considered the combined influence of spray cone angle and liquid film thickness to assess the nozzle atomization quality [34]. The expression is as follows:

$$\mathrm{SMD} = A\left(\frac{\sigma\mu_f^2}{\rho_g \Delta P^2}\right)^{0.25}\left(h_f \cos\left(\frac{\beta}{2}\right)\right)^{0.25} + B\left(\frac{\sigma\rho_f}{\rho_g \Delta P}\right)^{0.25}\left(h_f \cos\left(\frac{\beta}{2}\right)\right)^{0.75}, \quad (9)$$

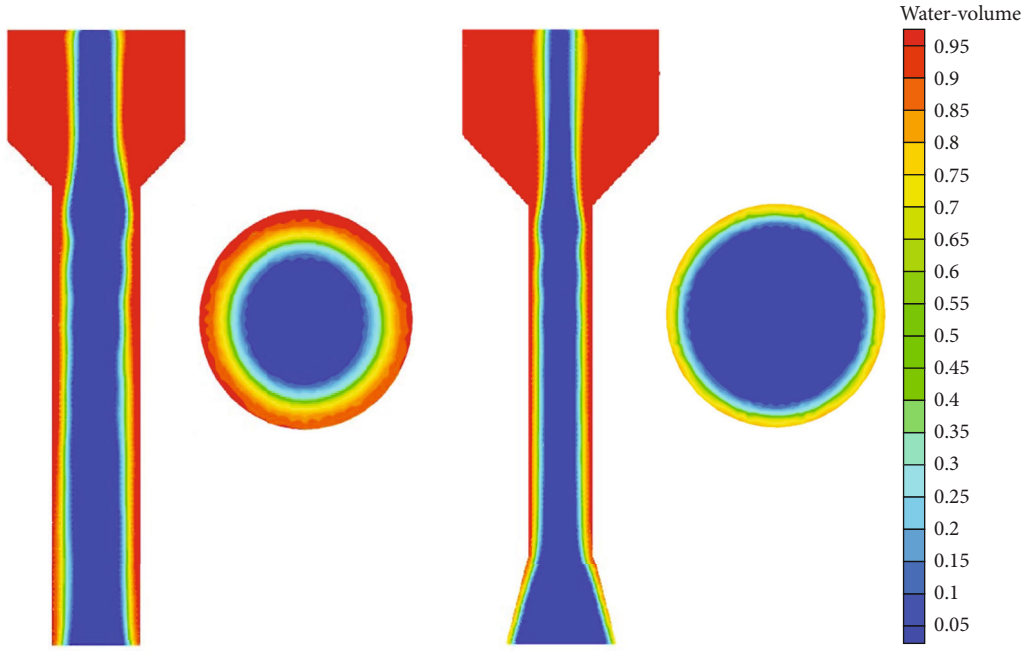

(a) Liquid phase volume fraction of $A_1B_2C_2D_2$ (b) Liquid phase volume fraction of $A_4B_1C_2D_4$

Figure 7: Cloud image of liquid phase volume fraction.

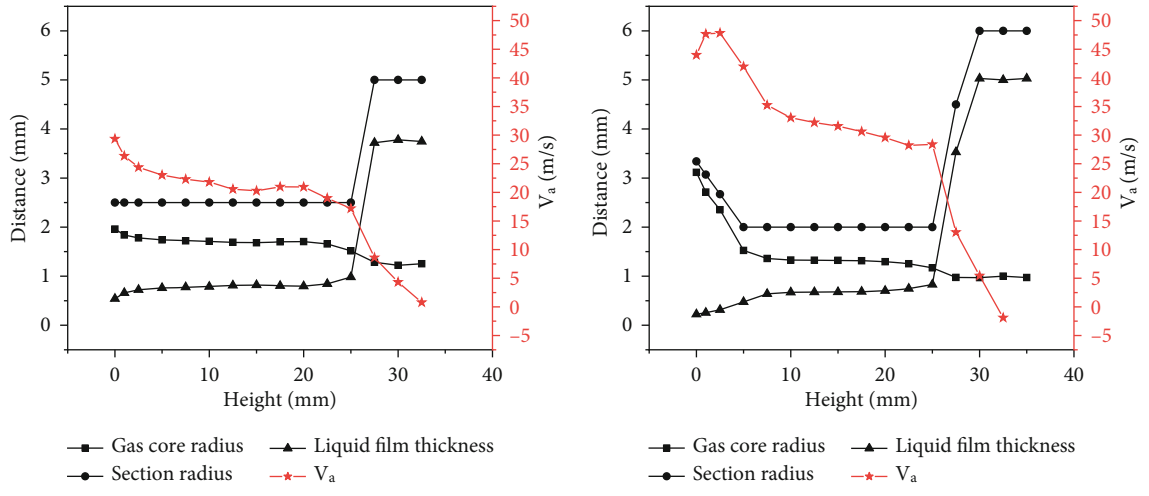

(a) $A_1B_2C_2D_2$ (b) $A_4B_1C_2D_4$

Figure 8: The relationship between gas core radius, section radius, and liquid film thickness with nozzle height.

where the values of A and B are related to the nozzle design structure, and their values can be calculated by the following formula:

$$A = 2.11\left[\cos\left(\frac{\beta}{2} - 30\right)\right]^{2.25}\left(\frac{3.4\times10^{-4}}{d_0}\right)^{0.4}, \quad (10)$$

$$B = 0.635\left[\cos\left(\frac{\beta}{2} - 30\right)\right]^{2.25}\left(\frac{3.4\times10^{-4}}{d_0}\right)^{0.2}, \quad (11)$$

where σ is surface tension, μ is liquid dynamic viscosity, and ΔP is inlet/outlet pressure difference.

Equation (9) is used to calculate the SMD of $A_1B_1C_2D_4$, $A_2B_1C_2D_4$, $A_3B_1C_2D_4$, and $A_4B_1C_2D_4$ with different expansion section angles. The SMD results are shown in Table 8.

Table 8 shows that the spray cone angle of $A_4B_1C_2D_4$ is 52.97°, the liquid film thickness of 0.250 mm is the smallest among all the nozzles, and the SMD is the smallest 40.52 μm. Compared with other optimized model nozzle, the atomization quality of $A_4B_1C_2D_4$ is better.

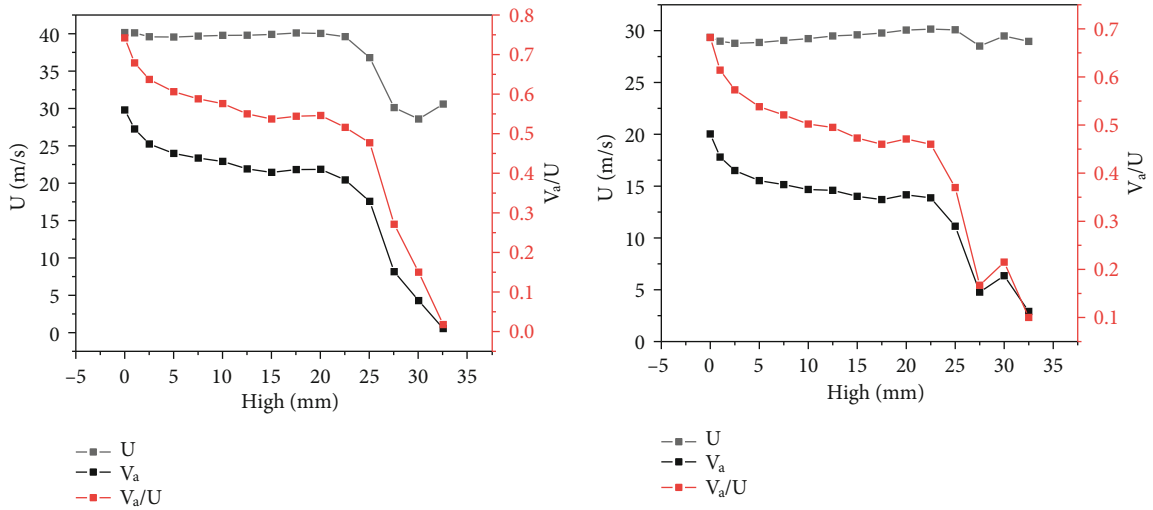

(a) $A_1B_2C_2D_2$ (b) $A_1B_4C_3D_2$

Figure 9: Variation of velocity as nozzle height at a gas volume fraction of 0.25.

Table 8: Comparison of atomization performance of optimization model.

Model	Atomizing cone angle/°	Liquid film thickness/mm	SMD/ μm
$A_1B_1C_2D_4$	87.57	0.595	53.34
$A_2B_1C_2D_4$	61.29	0.375	57.69
$A_3B_1C_2D_4$	54.03	0.288	46.44
$A_4B_1C_2D_4$	52.97	0.250	40.52

4. Conclusion

The influence of key structures of pressure swirl nozzles (swirl section diameter, contraction section angle, equal straight section diameter, and expansion section angle) on atomization quality is studied. Numerical simulation and orthogonal experiment are used to explore the variation law of spray cone angle and liquid film thickness with different nozzles.

(1) According to the orthogonal experiment results of spray cone angle, it can be concluded that primary and secondary factors influencing the spray cone angle are successive: expansion section angle, equal straight section diameter, swirl section diameter, and finally, contraction section angle. The structure combination with the largest spray cone angle is $A_1B_4C_3D_2$. As the expansion section angle increases, the spray cone angle decreases. With the increase of the equal straight section diameter, the spray cone angle increases. There is an optimum value for the contraction section angle. When the contraction section angle is 60°, the maximum spray cone angle is 73.77°

(2) According to the orthogonal experimental results of liquid film thickness, it can be concluded that the primary and secondary factors affecting the liquid film thickness are the expansion section angle, followed by the equal straight section diameter, and then, the contraction section angle and the swirl section diameter. The structural combination with the smallest liquid film thickness is $A_4B_1C_2D_4$. With the increase of the expansion section angle and the diameter of swirl section, the thickness of liquid film decreases gradually. When the equal straight section diameter increases, the thickness of the liquid film also increases. When the contraction section angle is 45°, the liquid film thickness reaches the minimum value of 0.449 mm

(3) The optimal structure combination of the nozzle is $A_4B_1C_2D_4$, whose spray cone angle, liquid film thickness, and SMD are 52.97°, 0.250 mm, and 40.52 μm, respectively. Compared with $A_1B_2C_2D_2$, the liquid film thickness is reduced by 0.405 mm, which improves the atomizing quality

Nomenclature

D_i: Tangential inlet diameter (mm)
D_s: Diameter of swirl chamber (mm)
L_s: Length of swirl chamber (mm)
α: Angle of contraction (°)
D_o: Diameter of equal straight section (mm)
L_o: Length of equal straight section (mm)
θ: Angle of expansion section (°)
L_k: Length of expansion section (mm)
VOF: Fluid volume fraction
φ: Volume fraction
u: Velocity (m/s)
ρ: Density (kg/m^3)
p: Pressure (N m^{-2})

μ: Dynamic viscosity (N·s/m^2)
g: Acceleration of gravity (m/s^2)
F: External volume force (N)
k, G_k, G_b: Turbulence kinetic energy
ε, Y_M: Turbulence diffusion rate
μ_{eff}: Effective viscosity (N·s/m^2)
S_k, S_ε: Source item
h_{lf}: Thickness film (mm)
r_w: Radius of the nozzle outlet (mm)
r_{ac}: Radius of the gas core (mm)
m: Mass flow rate (kg/s)
Δp: Pressure difference between inlet and outlet (N/m^2)
V_a: Axial velocity (m/s)
D: Nozzle diameter at the liquid film thickness section (mm)
U: Total velocity (m/s)
σ: Surface tension (N/m).

Data Availability

The data used to support the findings of this study are included within the article.

Conflicts of Interest

The authors declare that they have no conflicts of interest.

References

[1] Z. Tang, X. Huang, H. Zhao, and N. Yan, "Structural design and performance testing of fuel nozzles for aeroengine," *Tool engineering*, vol. 55, no. 10, pp. 95–95, 2021.

[2] T. Zhang, B. Dong, X. Zhou, L. Guan, L. Weizhong, and S. Zhou, "Experimental study of spray characteristics of kerosene-ethanol blends from a pressure-swirl nozzle," *International Journal of Aerospace Engineering*, vol. 2018, Article ID 2894908, 14 pages, 2018.

[3] Z. Guo, Y. Jin, K. Zhang et al., "Effect of low ambient pressure on spray cone angle of pressure swirl atomizer," *International Journal of Aerospace Engineering*, vol. 2021, Article ID 5539231, 10 pages, 2021.

[4] Z. Jiang, X. Feng, Y. Wang, and J. Chen, "Experimental analysis of atomization mechanism and influencing factors of air atomizing nozzle," *Journal of Central South University (Science and Technology)*, vol. 50, no. 10, pp. 2360–2367, 2019.

[5] Z. Sun, Z. Shen, and X. Li, "Experimental study on influence factors of atomization performance of air-blast lubricator," *Journal of Central South University (Science and Technology)*, vol. 49, no. 3, pp. 600–605, 2018.

[6] D. Zhang, Z. Li, W. Yi, and F. Wang, "Test study of spray characteristics of spiral nozzle in the spray tower," *Acta energiae solaris sinica*, vol. 34, no. 11, pp. 1969–1972, 2013.

[7] H. Lv, H. Liu, K. Han, C. Qi, and L. Zhang, "Theory and experimental research on spray characteristics of hollow cone nozzle for desalination," *Acta energiae solaris sinica*, vol. 41, no. 2, pp. 240–245, 2020.

[8] H. M. Gad, E. A. Baraya, T. M. Farag, and I. A. Ibrahim, "Effect of geometric parameters on spray characteristics of air assisted pressure swirl atomizer," *Alexandria Engineering Journal*, vol. 61, no. 7, pp. 5557–5571, 2022.

[9] F. Qingfei, B. Jia, L. Yang, and D. Minglong, "Effect of combustion chamber pressure pulsation on mixing ratio of liquid-liquid coaxial swirl injector," *Journal of aerospace power*, vol. 35, no. 2, pp. 294–297, 2020.

[10] Y. Lijun, F. Qingfei, X. Zhang, and Y. Wang, "Study on influence of configuration parameter of open-end swirl injector on its dynamics," *Journal of aerospace power*, vol. 22, no. 6, pp. 864–868, 2007.

[11] J. Liu, M. Sun, and Q. Li, "Analysis of geometric parameters influence on pressure swirl injector performance based on VOF interface tracking method," *Journal of aerospace power*, vol. 26, no. 12, pp. 2826–2833, 2011.

[12] K. Khani Aminjan, M. Heidari, D. D. Ganji, M. Aliakbari, F. Salehi, and M. Ghodrat, "Study of pressure-swirl atomizer with spiral path at design point and outside of design point," *Physics of Fluids*, vol. 33, no. 9, article 093305, 2021.

[13] K. Khani Aminjan, B. Kundu, and D. D. Ganji, "Study of pressure swirl atomizer with tangential input at design point and outside of design point," *Physics of Fluids*, vol. 32, no. 12, article 127113, 2020.

[14] X. Qiao, K. Li, and X. Zhu, "Effect of centrifugal nozzle structure on bio-oil spray characteristics," *Acta energiae solaris sinica*, vol. 40, no. 8, pp. 2097–2104, 2019.

[15] H. Pan, Z. Zhou, and L. Liu, "Influence of design parameters of the swirl nozzle on its spray characteristics," *Journal of mechanical engineering*, vol. 53, no. 2, pp. 199–206, 2017.

[16] L. Zhao, Y. Li, X. Zhu, and S. Shen, "Numerical analysis of structure parameter effects of a centrifugal nozzle on the spray characteristics," *Journal of Engineering Thermophysics*, vol. 40, no. 1, pp. 156–163, 2019.

[17] S. Zhen and F. Jiang, *Test Design and Data Processing*, China Building Materials Press, Beijing, 2004.

[18] G. Qiu, L. Hou, Z. Yi, L. Luo, and Y. Yunxia, "Effects of structure parameters of centrifugal nozzle on atomization performance," *Journal of propulsion technology*, vol. 41, no. 12, pp. 2782–2789, 2020.

[19] Y. Zhao, H. Yuan, C. Li, J. Zhao, and N. Mei, "Simulation study on ejection nozzle based on CFD orthogonal experiment," *Journal of Thermal Science and Technology*, vol. 16, no. 6, pp. 485–489, 2017.

[20] Q. Bai, W. Yang, and L. Hou, "Atomization characteristics analysis and structure optimization of an aviation fuel nozzle," *Journal of Shanghai Jiaotong University*, vol. 57, no. 1, pp. 84–92, 2022.

[21] Y. Song, *Investigation on the Flow Characteristics of Pressure Swirl Atomizer*, Nanjing university of aeronautics and astronautics, Nanjing, 2016.

[22] A. H. Lefebvre and M. Suyari, "Film thickness measurements in a simplex swirl atomizer," *Journal of Propulsion and Power*, vol. 2, no. 6, pp. 528–533, 1986.

[23] L. Wang, F. Bin, and G. Wang, "Process of pressure swirl nozzle atomization based on large eddy simulation," *Journal of propulsion technology*, vol. 42, no. 8, pp. 1855–1864, 2021.

[24] M. A. Zhao, M. Li, J. Suo, H. Feng, W. Liu, and S. Qiu, "Study on atomization characteristic and optimum design of a centrifugal nozzle," *Advances in aeronautical science and engineering*, vol. 8, no. 1, pp. 58–67, 2017.

[25] Y. Zhang, *Experiment and Numerical Studies on the Atomization of a Pressure Atomizer*, Chinese academy of sciences(Institute of engineering thermophysics), Beijing, 2013.

[26] L. Bayvel and Z. Orzechowski, *Liquid Atomization*, Taylor and Francis, London, 1993.

[27] A. Datta and S. K. Som, "Numerical prediction of air core diameter, coefficient of discharge and spray cone angle of a swirl spray pressure nozzle," *International Journal of Heat and Fluid Flow*, vol. 21, no. 4, pp. 412–419, 2000.

[28] F. Qingfei and L. Yang, "Visualization studies of the spray from swirl injectors under elevated ambient pressure," *Aerospace Science and Technology*, vol. 47, no. 2015, pp. 154–163, 2015.

[29] S. Yao, *Liquid Breakup and Atomization of Pressure Jet and Swirl Atomizers*, North Carolina State University, 2013.

[30] Q. Qiu, D. Jia, X. Zhu, X. Yi, and S. Shen, "Effect of structural parameters on film thickness at centrifugal nozzle outlet," *Journal of Jiangsu University (Nature science edition)*, vol. 36, no. 3, pp. 271–275, 2015.

[31] J. Liu, Q. Li, Z. Wang, and W. Haiyan, "Numerical simulation of flow field in pressure-swirl injector based on VOF interface tracking method," *Journal of aerospace power*, vol. 26, no. 9, pp. 1986–1994, 2011.

[32] J. Zhou, *Investigation on the Spray Characteristics of Pressure Swirl Atomizer with Different Internal Geometric Parameters*, Nanjing university of aeronautics and astronautics, Nanjing, 2020.

[33] Y. Lin and Y. Huang, *Combustion and Combustion Chamber*, Beihang University, Beijing, 2009.

[34] A. H. Lefebvre and X. F. Wang, "Mean drop sizes from pressure-swirl nozzles," *Journal of Propulsion and Power*, vol. 3, no. 1, pp. 11–18, 1987.